Biointerface Research in Applied Chemistry
Open-Access Journal (ISSN: 2069-5837)

Article
Volume 13, Issue 4, 2023, 351
https://doi.org/10.33263/BRIAC134.351

Spike Protein Potential Receptors Study: Comparative Computational Analysis Approach on SARS-CoV-2 - AC2/CD147 Complexes

Abdesselam. Makhloufi [1,2,*], Rima Ghemit [3], Meriem el Kolli [3]

[1] Laboratory of Biopharmacy and Pharmacotechnics . Ufas-1. Sétif, Algeria
[2] Industrial Engineering Department, Abbas Leghrour University, Khenchla, Algeria
[3] Laboratory of Chemical Process Engineering,, University of Ferhat Abbas, Setif-1, Algeria
* Correspondence: esssalim@yahoo.fr (A.M.);

Received: 17.06.2022; Accepted: 24.07.2022; Published: 17.09.2022

Abstract: SARS-CoV-2 invades host cells via interaction of its spike protein with the human angiotensin-converting enzyme 2 as the receptor. CD147, as a biomarker for hyperinflammation, was found to be the functional receptor for SARS-CoV-2 and an additional cell entry route. In this paper, we focused our analysis on the initial step of virus infection by comparing the affinity, stability, and specificity of the SARS-CoV-2 spike 1-AC2 and SARS-CoV-2 spike 1-CD147 complexes. Protein-protein docking was utilized for identifying the hotspot residues in the interface of spike protein with AC2 and CD147. The results of binding free energies showed a high affinity of SP1-AC2 complex (-52.97 kcal/mol) compared with SP1-CoV2/CD147 (-35.75 kcal/mol). RMSF values indicate that the spike protein of SARS-CoV-2 RBD is more compatible with binding to the human ACE2 with high flexibility. Computational analysis of binding modes and protein contacts reported that CD147 and ACE2 might be two complementary receptors mediating virus infection and confirmed the experimental results previously.

Keywords: SARS-COV-2 S-protein target; protein-protein interactions; molecular dynamic simulation.

1. Introduction

Since its first appearance in December 2019, the severe acute respiratory syndrome coronavirus-2 (SARS-CoV-2) pandemic has had a major impact on the health of millions of people and the global economy [1]. The number of infected and dead is rising, accompanied by highly transmissible variants of SARS-CoV-2 [2]. Conversely, no approved vaccine or cure is available to treat this infectio[n [3,4], so there is an urgent need to provide insight into disease and pathogens or discover new and safe drugs/vaccines against complex diseases.

The coronavirus virion is made up of nucleocapsid (N), membrane (M), envelope (E), and spike (S) proteins [5-7], which are structural proteins. CoV entry into host cells is mediated by its transmembrane spike (S) glycoprotein, and the angiotensin-converting enzyme 2 (ACE2) has been identified as a cellular receptor [8-10]. ACE2 is an enzyme that activates angiotensin, a peptide hormone involved in controlling blood pressure, with diverse physiological and pathological functions in cardiovascular, intestinal, renal, and respiratory systems—making these cells the primary targets for infection by the virus [11-14]. An in-depth study has discovered another novel route for SARS-CoV-2 infection. Wang *et al*. suggested that CD147,

which is present on the surface of T lymphocytes, can provide an additional entry for SARS-CoV-2 infection through binding to the viral spike (S) protein [15]. CD147, a receptor on host cells also known as Basigin (basic immunoglobulin) or EMMPRIN (extracellular matrix metalloproteinase inducer), is a transmembrane glycoprotein that contributes to the development of tumors, invasion of Plasmodium and infection mediated by bacteria or viruses [16,17]. The crucial role of the binding mechanism between the SARS-CoV-2 virus Spike protein receptor binding domain (RBD) and its receptors is in the infection initiation process. A study of the viral glycoprotein and their host's interactions with AC2 and/or CD147 is of critical importance for a better understanding of virus entry into cells. It emphasizes the importance of these receptors in the spread of COVID-19 [18].

In the current work, we focused our study on predicting the binding affinity and specificity of protein-protein interactions. The computational approaches, including molecular docking and dynamics simulation of both complexes SARS-CoV-2 spike 1-AC2 (complex-1) and SARS-CoV-2 spike 1-CD147 (complex-2), were carried out, so the main objective of the present study was to examine the difference between entry mechanisms via ACE2 and CD147 receptors, which will contribute to a deeper understanding the dynamics of the SARS-CoV-2 pandemic and supplied a theoretical basis for guiding clinical decision-making.

2. Materials and Methods

2.1. Materials, data set.

The crystallized structure of the angiotensin-converting enzyme-related carboxypeptidase ACE2 receptor [1R4L] [19], CD147 [5X0T] [20], and the SARS-CoV-2 RBD [6W41] [21] were downloaded from the RCSB Protein Data Bank (PDB) (https://www.rcsb.org/). 1R4L and 6W41 files are possessed for each of the three chains. Chain A corresponded to human ACE2, and chain C of RBD of monomeric chain spike protein were selected and analyzed via Discovery Studio software for further investigation [22].

2.2. Proteins preparation.

The initial structures were checked for errors and prepared within MOE software (Molecular Operating Environment (MOE), 2015) [23]. First, the proteins were prepared by correcting the missing bonds, which were broken in X-ray diffraction, then the hydrogen atoms were added. After that, the three proteins were minimized individually in the same software.

2.2.1. Molecular docking procedure.

The molecular docking of the selected proteins was carried out by different online docking servers. Firstly, the docked protein-protein complexes were scored with HDOCK server (http://hdock.phys.hust.edu. cn/), which is based on a hybrid algorithm of template-based modeling and ab initio free docking. Moreover, Hdock also supports protein-RNA/DNA docking with an intrinsic scoring function [24,25].

Moreover, the HAWKDOCK server has been used to predict protein-protein interaction between SP1of SARS-CoV-2 RBD with AC2 and CD147. The Hawkdock, a free and open-accessed web server (http://cadd.zju.edu.cn/hawkdock/), was developed to predict and analyze the structures of Protein-protein interactions (PPIs). That combines the HawkRank program for re-ranking docking poses and several third-party programs, including ATTRACT for protein-

protein docking, MM/GBSA for the identification of key residues, and 3Dmol.js for molecular visualization [26].In this run, both proteins were uploaded, and default server parameters were used. The top 10 models were downloaded, the model 1 (top model) was taken for further analysis based on scoring value.

The protein-protein interactions (PPIs) were also evaluated with another web server, employing a molecular docking webserver, High Ambiguity Driven protein-protein Docking HADDOCK 2.4 (https://wenmr.science.uu.nl/haddock2.4/) is an integrative platform developed by Prof Alexander Bonvin at Utrecht University as a modeling tool to predict protein-protein interactions within biomolecular complexes [27]. CPORT (http://haddock.chem.uu.nl/services/cport/) web server was used to determine the active site (and passive) of the proteins. The obtained complexes were processed and analyzed through the PRODIGY tool (https://wenmr.science.uu.nl/prodigy/) [28]. PDBEPISA server (http://www.ebi.ac.uk/pdbe/prot_int/pistart.html) was used to investigate the structure energies and residue-residue interactions [29]. The Interface visualization of the protein-protein complexes interactions was analyzed using the PyMol package [30].

2.2.2. Molecular dynamics procedure.

Furthermore, the study of the dynamics of protein-protein interactions was carried out using CABS Flex 2.0 online simulation server (http://biocomp.chem.uw.edu.pl/CABSflex2), which predicts fluctuations and protein aggregation propensity [31]. For 10 ns, the distance restraints generator was set to default values. The number of cycles and trajectory frames was set to 50, with a global weight of 1.0 and a temperature of 1.4. The root-mean-square fluctuations and contact maps were obtained.

3. Results and Discussion

3.1. Molecular docking studies.

3.1.1. Protein-protein Dockscoring.

First, the complex interactions were computed by employing the protein-protein docking approach using the HDOCK server.

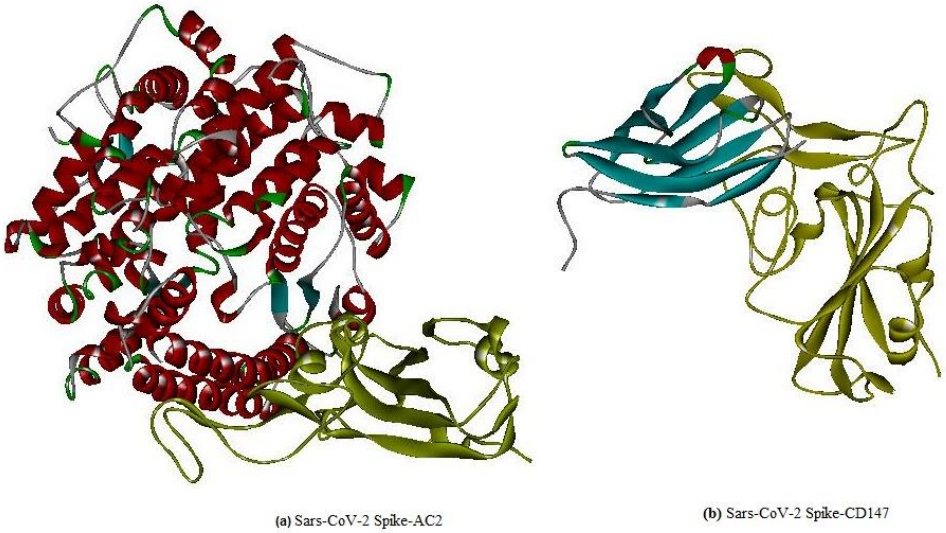

Figure 1. Docking of SARS-CoV-2 RBD (yellow cartoon) cartoon) against AC2 (red cartoon) and CD147 (cyan cartoon) receptors using HDOCK server.

Model 1 was selected for further analysis with the lowest docking of each complex. The docking score for the SARS-CoV-2/AC2 was 345.14kcal/ mol and -251.34 kcal/mol for the SARS-CoV-2/CD147. The root-mean-square deviation (RMSD) values were 0.6 and 71.92 Å for the complex-1 and -2, respectively. The main interaction region of SARS-CoV-2 RBD with the two receptors was found in the range of 400 and 505.

As it appears in Table 1, the common amino acid residues of the targeted site of 2019-nCoV are LYS-417, TYR-453, ALA-475, and ASN-487. Moreover, SP1 of SARS-CoV-2 could interact with receptors with two bonds, LEU-455 and TYR-449 to AC2, and with TYR-473, ASN-487, TYR-505, and ALA-475 (three bonds) to CD147.

Table 1. Interaction residues of both complexes within < 3 A° regions.

Sars-CoV-2 Spike-AC2	Sars-CoV-2 Spike-CD147
LYS-417 – LYS-31, TYR-449 – ASP-38	ASP-405 – HIS-115, THR-415 – SER-113
TYR-449 – GLN-42, TYR-453 – HIS-34	LYS-417 – GLU-114, LYS-417 – MET-123
LEU-455 – HIS-34, LEU-455 – ASP-30	ASP-420 – LYS-111, TYR-421 – MET-123
ALA-475 – GLN-24, GLU-484 – LYS-31	TYR-421 – LYS-111, TYR-453 – GLU-120
ASN-487 – ASP-30, PHE-486 - TYR-83	PHE-456 – HIS-170, LYS-458 – ARG-166
PHE-486 – LYS-353, TYR-489 – TYR-83	TYR-473 – GLU-168, TYR-473 – HIS-170
GLN-498 – LYS-353, GLN-493 – GLU-35	GLN- 474– SER-161, ALA-475 – ASN-152
THR-500 – ASN- 330	ALA-475 – VAL-160, ALA-475 – HIS-170
	ASN-487 – PHE-159, ASN-487– ASN-152
	TYR- 505 – ASN-117, TYR- 505 – HIS-205

3.1.2. Binding free energy properties of complexes.

To predict the free intermolecular binding energy of protein-protein interactions. The complexes were crosschecked further on other platforms: HAWKDOCK, via MM/GBSA methodology. The molecular mechanics energies combined with the generalized Born and surface area (MM/GBSA) method are widely used to predict binding free energies and to identify the correct binding conformations in the protein-protein complex, which are more theoretically rigorous than scoring functions. Furthermore, MM/GBSA with per-residue energy decomposition of the binding free energy of a protein-protein complex has been successfully employed to highlight the key residues in the binding interface. The binding interactions of each residue–residue pair consist of the following four energy components: VdW: Vander Waal potentials, ELE: Electrostatic potentials, GB: Polar Solvation, and SA: Nonpolar contribution to the solvation. TOTAL: Final estimated binding free energy was calculated from the terms above. In Table 2, the top ten scoring complexes were resumed.

Table 2. Scoring and docking energy (in kcal/mol) values for models generated by hawkdDock.

Sars-CoV-2 Spike-AC2		Sars-CoV-2 Spike-CD147	
Rank	**Score**	**Rank**	**Score**
1	6472.23	1	-4364.16
2	5532.83	2	-4168.96
3	5357.35	3	-3998.97
4	5309.49	4	-3915.86
5	5186.02	5	-3904.77
6	5167.92	6	-3895.86
7	5140.37	7	-3844.02
8	5116.06	8	-3843.80
9	5108.53	9	-3825.36
10	4922.5	10	-3752.60

From the MM-GBSA results presented in Table 3, the complex RBD of SARS-CoV-2/AC2 revealed an importantly low binding free energy -52.97 kcal/mol than that of RBD of SARS-CoV-2/CD147 -35.96 kcal/mol. The contribution of van der Waals energy and electrostatic energy was observed to be -158.21/-807.12kcal/mol and -83.21/-135.78kcal/mol, respectively.

Table 3. A comparison between the binding free energy of complexes using the MM-GBSA program in HawkDock server.

	Sars-CoV-2 Spike-AC2	**Sars-CoV-2 Spike-AC2**
VdW	-158.21	-83.21
ELE	-807.12	-135.78
GB	932.02	194.33
SA	-19.66	-11.30
TOTAL	-52.97	-35.96

MM-GBSA is a high-throughput virtual screening approach widely used to estimate the free binding energy of the protein-ligand or protein-protein/peptide complexes. MM-GBSA allowed us to assign each amino acid's contribution to each protein's interface.

The most significant hotspot residues of the SARS-CoV-2 Spike-AC2 complex are illustrated in Figure 2. LYS-130, ILE-136, THR-138, ARG-25, and SER-137 have been considered the hotspots residues of SARS-CoV-2 RBD, and SER-137, LEU-138, TRP-310, VAL-280, and GLN-287 for AC2.

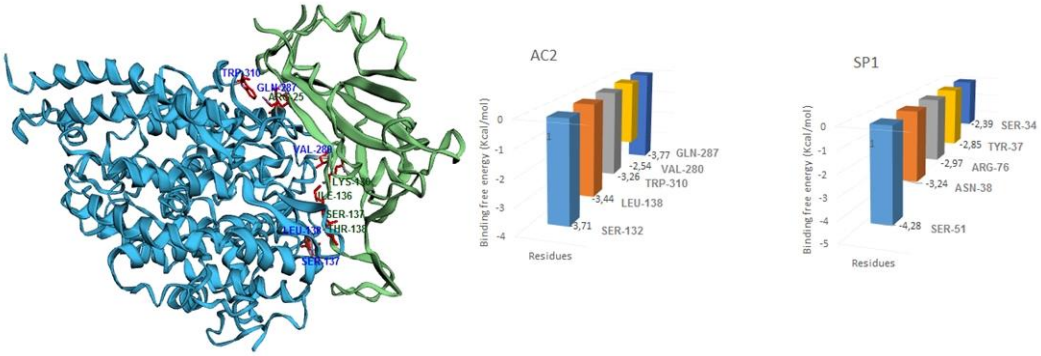

Figure 2. Analyzing interactions of the top five amino acid residues and its binding free energy score of SARS-CoV-2 RBD-ACE2 complex.

On the other hand, as seen in Figure 3, the interacting amino acid interface of spike protein with CD147 are SER-51, ASN-38, ARG-76, TYR-37, and SER-34. Hotspots for CD147 are ILE-100, LEU-4, ARG-104, THR-102, and SER-96.

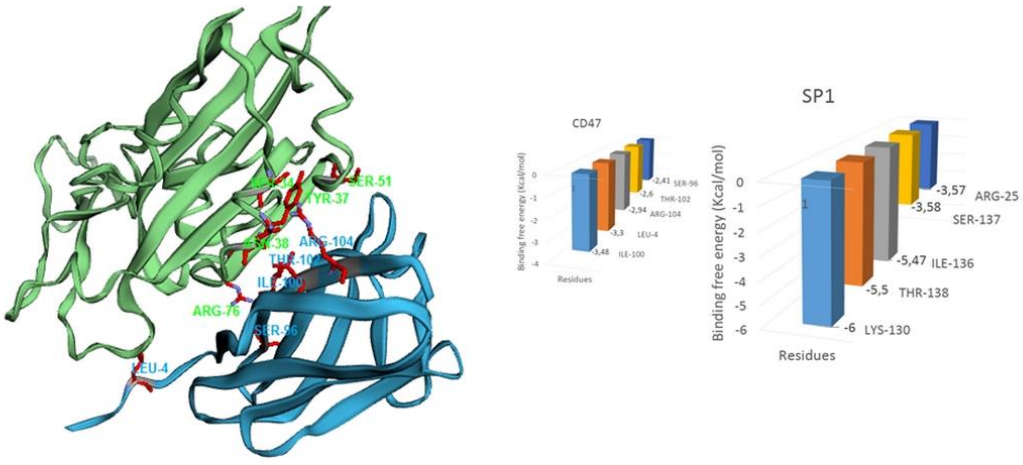

Figure 3. Analyzing interactions of the top five amino acid residues and its binding free energy score of SARS-CoV-2 RBD-CD147 complex.

3.1.3. Protein-protein binding affinity prediction.

Another simulation docking method has been used, HADDOCK 2.4 sever; the tool combines Coulomb electrostatic energies, non-bonded intermolecular Van der Waals, empirically derived desolvation energies, and buried surface area. The interactions between the spike protein with ACE2 and CD147 complexes were compared with the HADDOCK 2.4 web server, followed by further interaction analysis with PRODIGY. Active residues were defined for the server to be considered as restraints by the CPORT algorithm. The amino acids surrounding the active residues of both proteins were selected as passive in the docking procedure.

Table 3. Predicted (active residues) and surrounding residues (passive residues) by the CPORT algorithm.

Protein	Active residues	Passive residues
SARS-CoV-2 RBD SP1	343, 357, 359, 360, 366, 367, 369, 370, 371, 372, 373, 374, 375, 377, 386, 390, 391, 396, 430, 441, 444, 445, 449, 452, 455, 456, 470, 471, 474, 475, 477, 478, 479, 480, 481, 482, 483, 484, 485, 486, 487, 489, 490, 492, 493, 499, 500, 516, 517, 518, 519, 520, 521, 522, 523, 525, 527	333, 334, 335, 336, 337, 339, 340, 344, 345, 346, 347, 351, 352, 355, 356, 362, 364, 376, 378, 379, 380, 381, 382, 383, 384, 385, 388, 389, 417, 421, 426, 427, 428, 429, 436, 437, 439, 440, 443, 446, 447, 450, 457, 458, 464, 467, 468, 469, 472, 473, 476, 494, 496, 498, 501, 502, 506, 515, 526.
AC2	21, 81, 82, 84, 85, 86, 87, 88, 94, 98, 101, 156, 157, 159, 246, 249, 250, 251, 253, 254, 255, 257, 258, 259, 610, 611, 612, 613, 615.	19, 20, 23, 24, 26, 78, 79, 89, 90, 91, 92, 93, 95, 99, 102, 103, 104, 151, 154, 160, 162, 163, 210, 211, 247, 256, 281, 482, 490, 491, 492, 493, 602, 603, 605, 606, 607, 608, 609, 614.
CD147	98, 99, 100, 101, 102, 103, 104, 106, 114, 115, 116, 117, 118, 119, 120, 121, 123, 127, 129, 130, 131, 132, 133, 135, 157, 165, 190, 191, 192, 204, 205.	105, 108, 109, 110, 111, 112, 113, 125, 128, 136, 137, 151, 153, 154, 155, 156, 159, 162, 163, 164, 166, 168, 170, 172, 173, 175, 176, 177, 188, 189, 193, 194, 195, 196, 199, 201, 202, 203.

For the first run, HADDOCK clustered 103 structures in 12 clusters for complex-1 and 123 structures in 17 clusters for complex-2. The model with the lowest HADDOCK score has been selected for further studies for each complex. The average HADDOCK score for the SP1-AC2 was -25.6 +/- 22.8 and -17.3 +/- 14.5 for SP1-CD147. The Root Mean Square Deviation (RMSD) value of SP1-AC2 was found to be 0.5-0.7 Å and 5.7-0.2 Å for SP1-CD147, which indicates the reliability of the docking protocol. The buried surface area of the first complex, 3115.0 +/- 336.0 $Å^2$, was also higher than the second, 2309.1 +/- 94.8 $Å^2$.

Table 4. Energetic calculations with HADDOCK. vdW: van der Waals interaction score; Elec: electrostatic interaction score; Desol: desolvation score; BSA: buried surface area.

Complex	Haddock Score	vdW (a.u.)	Elec (a.u.)	Desol (a.u.)	BSA ($Å^2$)	RMSD
SP1-AC2	-25.6 +/- 22.8	-81.8 +/- 14.0	-548.2 +/- 86.8	35.5 +/- 0.3	3115.0 +/- 336.0	0.7 +/- 0.5
SP1-CD147	-17.3 +/- 14.5	-84.2 +/- 7.5	-182.9 +/- 31.3	1.3 +/- 3.6	2309.1 +/- 94.8	5.7 +/- 0.2

Furthermore, the best cluster of AC2 and CD147 in complex with S protein were further examined by PRODIGY. Finally, the complex stability was measured through the dissociation constant Kd.

The number and the characteristics of these protein-protein interactions are shown in Table 5. The complex of SARS-CoV-2 RBD with AC2 showed a ΔG value of -16.1 kcal mol^{-1}, which is higher than those observed in the complex with CD147 -11.1 kcal mol^{-1}. The predicted dissociation constant (KD) of SP1-AC2 value was 1.6E-12, smaller than SP1-CD147 7.6E-09, which confirms the strong binding affinity and high stability between RBD and AC2 with respect to the CD147.

Table 5. Binding affinity and Kd prediction in protein-protein interactions by PRODIGY server.

Complex	Binding energy (kcal/mol ΔG	Charged-charged	Charged-polar	Charged-apolar	Polar-polar	Polar-apolar	Apolar-apolar	Kd (M) at 25.0 °C
SP1-AC2	-16.1	30	29	39	13	17	14	1.6E-12
SP1-CD147	-11.1	15	21	22	10	15	14	7.6E-09

Next, the hydrogen bonding and salt-bridge interactions at the protein-protein interface were analyzed by using the PDBePISA server. Details of these chemical interactions are given in Table 6.

Figure 4 and Table 6 provide the intermolecular protein-protein interactions and surface interface areas of the docked complexes. Complex interactions showed an interface area of 1693.3Å^2 in SP1-AC2 and 1146.5 Å^2 in the SP1-CD147 complex.

Table 6. Parameters of the interface of the interactions between spike protein AC2 and CD147 predicted by PDBePISA server.

		Protein		Complex		
		Interface Residues	**Interface Surface (A^2)**	**Interface Surface (A^2)**	**N_{HB}**	**N_{SB}**
SP1-AC2 Complex	**Spike**	55	10476	1693.3	21	12
	AC2	54	24412			
SP1-CD147 Complex	**Spike**	35	10517	1146.5	14	1
	CD147	6533	6533			

The structural comparison of the amino acids at the interface revealed that the spike protein interacts with ACE2 with 21 hydrogen bonds and 12 salt bridges. For the second complex, spike protein showed (to CD147) 14 hydrogen bonds and 1 salt bridge. This explains why the SP1 bonded with high affinity to the AC2 and not at the same value as the CD147.

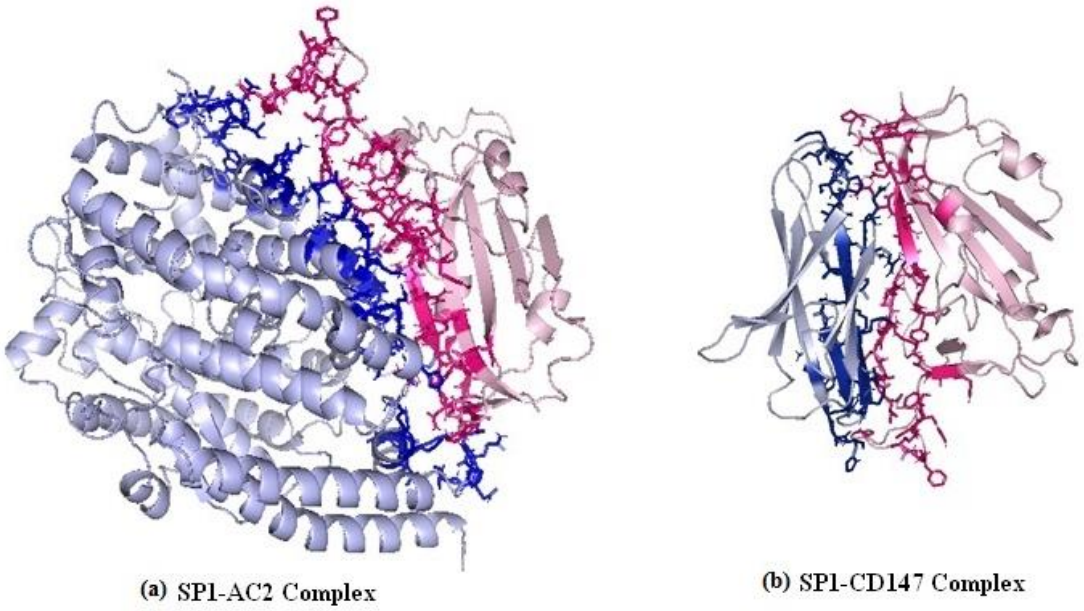

Figure 4. **(a)** the interface interaction residues between the SARS-CoV-2 RBM (in red) and ACE2 (in blue). **(b)** The interface interaction between SARS-CoV RBM (in red) and CD147 (in blue).

The salt bridges in the first complex were found to be extremely important in binding SP1 to ACE2. The residue Arg-357 and GLU-238 of spike protein interacted with two sites to

ARG-466 and GLU-467 of ACE2, respectively, LYS-458 formed two bonds to ASP-216 and one to ASP-213 residue.

Table 7. Hydrogen bond and Salt-bridge in the interface interactions residues of both complexes.

	SP1-AC2	Distance (Å)	SP1-CD147	Distance (Å)
Hydrogen-bond	CYS-480–LYS-94	2.27	GLU-484–HIS-195	3.61
	ASN-481–LYS-94	1.77	GLU-340–LYS-475	2.57
	SER-469–ARG-219	2.82	LYS-356–GLU-483	2.59
	THR-470–ARG-219	2.37	LYS-356–GLU-479	3.76
	TYR-396–LYS-234	1.83	ARG-357–GLU-238	3.81
	GLU-340–LYS-475	1.73	ARG-357–GLU-238	2.66
	ASN-360–SER-607	3.79	ARG-457–GLU-224	3.42
	SER-359–THR-608	3.88	LYS-458–ASP-216	2.67
	TYR-351–GLU-197	1.65	LYS-458–ASP-213	2.55
	LYS-356–GLU-483	1.61	LYS-458–ASP-216	2.72
	ARG-357–GLU-483	2.83	ARG-466–GLU-467	3.53
	ARG-357–GLU-483	2.19	ARG-466–GLU-467	2.64
	ARG-357–GLU-238	1.69		
	LYS-458–ASP-216	1.71		
	LYS-458–ASP-213	1.54		
	ARG-466–GL-224	3.70		
	ARG-466–GLU-467	1.70		
	THR-470–GLU-197	3.46		
	THR-470–ASP-201	3.06		
	ASN-481–LEU-85	2.75		
	ASN-481–PRO- 84	2.36		
Salt-bridge	GLU-484–HIS-195	3.61	ASP 46-ARG 166	2.90
	GLU-340–LYS-475	2.57		
	LYS-356–GLU-483	2.59		
	LYS-356–GLU-479	3.76		
	ARG-357–GLU-238	3.81		
	ARG-357–GLU-238	2.66		
	ARG-457-GLU-224	3.42		
	LYS-458–ASP-216	2.67		
	LYS-458–ASP-213	2.55		
	LYS-458–ASP-216	2.72		
	ARG-466–GLU-467	3.53		
	ARG-466–GLU-467	2.64		

While for the hydrogen bonds, ARG- 357 of SP1 tended to interact with GLU 483 (two bonds) and GLU -238. In the second complex, the residues critically involved in an interaction was the ARG 357 with two hydrogen bonds to GLU-114 and one to HIS-115. Further detailed information is listed in Table 7.

On the other hand, a comparison of the predicted binding sites (hydrogen bonds) of the complexes demonstrated that the common interactive residues of SP1 in the two complexes include: ASN-360, SER-359, TYR-351, LYS-356, and ARG-357. The hydrogen bonds and salt bridge interactions play an important role in the stability of the protein-protein formation, which justifies the different results of the binding interactions obtained in the investigated complexes.

3.2. Molecular dynamics simulations analysis.

To examine the fluctuation of the respective amino acids in the individual complex and their respective conformational stability. The complex interactions were further evaluated via the CABS-flex 2.0 server. Ten (10) different models were predicted by the exploratory simulation per run; the first model of each was selected based on its best structural heterogeneity and stability.

Root Mean Square Fluctuations plots of protein residues fluctuation and aggregation are illustrated in Figures 5, 6, and 7. Flexibility enhancement can be observed in the average interatomic distances between the atoms.

From these results, The RMSF of this simulation was found to be between 0.081 and 5.98 Å for the first complex and from 0.11 to 5.13 Å for the second. In short analysis, the RMSF plot indicates the structural stability of the SP1-AC2 complex is more stable than SP1-CD47.

In both complexes, for loops (residues 362-389 441–446, 475-480, and 500–503) of the SARS-CoV-2 S protein RBD make contact with ACE2. In the SARS-CoV-2-CD47 simulations, the loops formed by residues 363-391, 442–447, 475-485, and 499–503. The maximum fluctuation was observed at residue 227, while the minimum was displayed between 39–59. In the case of SARS-CoV-2 S RBD alone (did not bind), the fluctuations exhibited higher values between 458-467, 479-483, and 500-503 residues (Figure 5).

Furthermore, the comparison of the RMSF plot of the SP1 single with the corresponding both complexes, interestingly, in the range between 458-467, 479-483, and 500-503 residues (region of loops) exhibited higher fluctuations when not bounded bound to ACE2 and CD47.

Higher RMSF values indicate more protein flexibility, whereas the lowest value implies the limited motion of the system during the simulation process in relation to its average position.

The spike protein values of these segments in complex-1 are significantly lower than the SP1 CD47 in complex-2, indicating stabilization upon complex-1 formation. Except for this spike, protein displayed increasing RMSF fluctuation values at residue numbers 442, 443, and 444 with a fluctuation of 5.324, 5.756, and 5.988 A°, respectively.

From the graph in Figure 5, we can notice an overall decrease in the fluctuation at 478-484 spike protein residues compared to the same protein without ACE2 or CD147 in the same region. It would seem that this region in S protein RBD of SARS-CoV-2 is more effectively stabilized after binding to their two receptors. This agrees with HADDOCK docking studies; almost the Hydrogen bond and Salt-bridge in the interface interactions protein-protein looked at this region, particularly in the first complex.

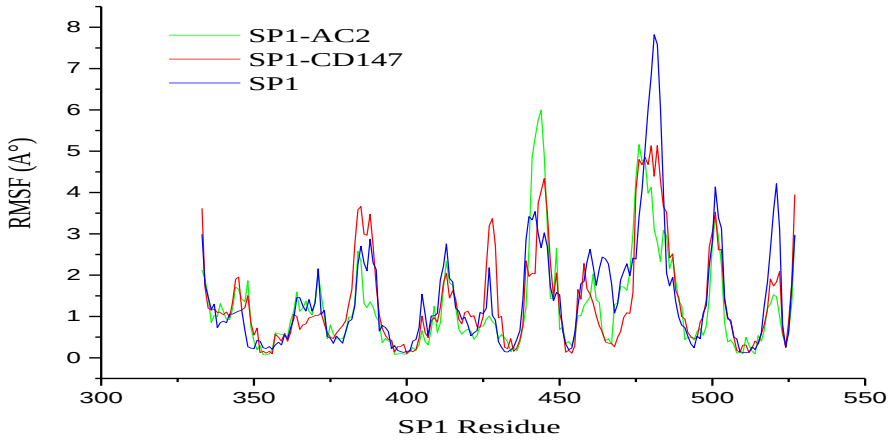

Figure 5. Root mean square fluctuation (RMSF) of spike (S) protein RBD bound to ACE2 (in green), bound to CD147 (in red), and unbound (in blue).

To describe in more detail of the conformational changes, the simulations of single AC2 and CD47 structures were also performed. As seen in Figures 6 and 7, significant changes were noticed in the structural flexibility of ACE2 (in complex-1). Fluctuations of this protein appeared in the threshold of 1-3 Å (Figure 6), confirming this conformation's stability. Furthermore, the contact map presented an interaction interface between all the atoms in the ACE2 complex.

Whereas the lower RMSF values associated with the bindings of CD47 with SP1 (Figure 7) did not produce a significant difference compared with the RMSF of CD47 alone and could suggest a limited fluctuation of the complex in the process of the simulation.

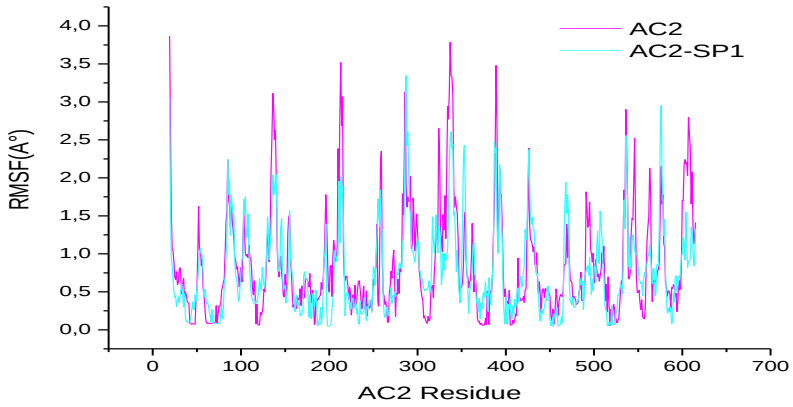

Figure 6. Root mean square fluctuation (RMSF) of ACE2 unbound (in pink) and bound to spike (S) protein RBD (in cyan).

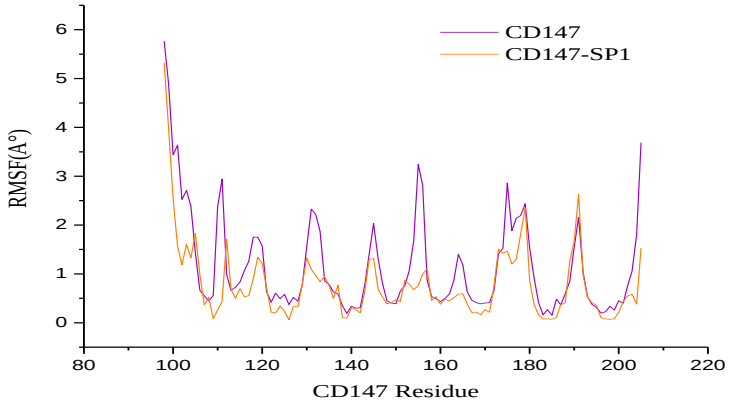

Figure 7. Root mean square fluctuation (RMSF) of CD147 unbound (in purple) and bound to spike (S) protein RBD (in red).

4. Conclusions

From this computational analysis approach through protein-protein docking and MD simulations, the aim of the present research was to examine the binding of SARS-CoV-2 receptors, ACE2 and or CD147, or both. The docking ranking results in this study showed that the AC2 receptor revealed a powerful target on the RBD spike protein of SARS-CoV-2. The larger number of interactions in the SARS-CoV-2-AC2 complex also translated to a notably higher ΔGbind, computed via the MM-GBSA method. In addition, our data displayed that CD147 serves as an alternative entry receptor for viral entry. Although the weak binding affinity and low stability with respect to the AC2. In order to further validate the findings of

our docking results, we used molecular dynamics simulation studies of both complexes. Based on the RMSF values, both complexes were stable without obvious fluctuations. These results validated the docking interaction analysis and endorsed that CD147 can strongly bind with SARS-CoV-2. Our trajectories analysis of binding modes and protein contacts reported that CD147 and ACE2 might be two complementary receptors in mediating virus infection.

Funding

This research received no external funding.

Acknowledgments

Declared none.

Conflicts of Interest

The authors declare no conflict of interest.

References

1. Synowiec, A.; Szczepański, A.; Barreto, E.; Lie, L.K.; Pyrc, K. Severe Acute Respiratory Syndrome Coronavirus 2 (SARS-CoV-2): a Systemic Infection. *Clin. Microbiol. Rev.* **2021**, *34*, 00133-20, https://doi.org/10.1128/CMR.00133-20 .
2. Shanab, J.; Wangab, W.; Zhangab, S.; Huana, Q. Evidence for a mouse origin of the SARS-CoV-2 Omicron variant. *J. Genet. Genomics.* **2021**, 48, 1111-1121, https://doi.org/10.1016/j.jgg.2021.12.003.
3. Ur Rehman, S.; Ur Rehman, S.; Yoo, H. COVID-19 challenges and its therapeutics. *Biomed. Pharmacother.* **2021**, *11*, 142, https://doi.org/10.1016/j.biopha.2021.112015 .
4. Peter, J. *et al*. Global public health security and justice for vaccines and therapeutics in the COVID-19 pandemic. *EClinicalMedicine.* **2021**, *39*, 101053, https://doi.org/10.1016/j.eclinm.2021.101053 .
5. Wu, S.; Tian, C.; Liu, P.; Guo, D.; Zheng,W.; Huang, X.; Zhang,Y.; Liu, L. Effects of SARS-CoV-2 mutations on protein structures and intraviral protein–protein interactions. *J. Med. Virol*. **2021**, 93, 2132-2140, https://doi.org/10.1002/jmv.26597 .
6. Yesudhas, D.; Srivastava, A.; Gromiha, M.M. COVID-19 outbreak: history, mechanism, transmission, structural studies and therapeutics. *Infection*. **2021**, *49*, 199–213, https://doi.org/10.1007/s15010-020-01516-2 .
7. Gaoa, X.; Chen, B.; Zhu, K.; Kaixiang, Pengjiao, H.; Wang, M.; Cui, S. Crystal structure of SARS-CoV-2 papain-like protease. *Acta Pharm. Sin. B.* **2021**, *11*, 237-245, https://doi.org/10.1016/j.apsb.2020.08.014 .
8. Low-Gan, J.; Huang, R.; Kelley, A.; Warner Jenkins, G.; McGregor, D.; Van Smider, V. Diversity of ACE2 and its interaction with SARS-CoV-2 receptor binding domain. *Biochem. J.* **2021**, *19*, 3671-3684, https://doi.org/10.1042/BCJ20200908 .
9. Lia, Z.; Zhang, J.Z.H. Quantitative analysis of ACE2 binding to coronavirus spike proteins: SARS-CoV-2 vs. SARS-CoV and RaTG13. *Chem. Phys*. **2021**, *23*, 13926-13933, https://doi.org/10.1039/D1CP01075A.
10. Warner, F.J.; Smith, A. I.; Hooper, N.M.; Turner, A. J. a Angiotensin-converting enzyme-2: a molecular and cellular Perspective CMLS. *Cell. Mol. Life Sci.* **2004**, *61*, 586-590, https://doi.org/10.1007/s00018-004-4240-7 .
11. H. Zhang, J.M. Penninger, Y. Zhong, A. Slutsky, Angiotensin-converting enzyme 2 (ACE2) as a SARS-CoV-2 receptor: molecular mechanisms and potential therapeutic target. *Intensive Care Med.* **2020**, *46*, 586-590, https://doi.org/10.1007/s00134-020-05985-9 .
12. Hede, G. ACE2 as Drug Target of COVID-19 Virus Treatment, Simplified Updated Review. *Int. J. Pept.* **2021**, *8*, https://doi.org/10.29252/rbmb.9.1.97 .
13. Beyerstedt, S.; Casaro, B.; Bevilaqua, E. COVID-19: angiotensin-converting enzyme 2 (ACE2) expression and tissue susceptibility to SARS-CoV-2. *Eur. J. Clin. Microbiol. Infect. Dis*. **2021**, *40*, 905–919, https://doi.org/10.1007/s10096-020-04138-6 .

14. Van Lier, D.; Kox, M.; Santos, K.; Van der Hoeven, H.; Pillay, J.; Pickkers, P. ACE2, Increased blood angiotensin converting enzyme 2 activity in critically ill COVID-19 patients. *Open Research.* **2021**, *7*, 00848, https://doi.org/10.1183/23120541.00848-2020.
15. Fenizia, C. *et al*. SARS-CoV-2 Entry: At the Crossroads of CD147 and ACE2. *Cells*. **2021**, *10*, 1434, https://doi.org/10.3390/cells10061434 .
16. Shilts, A.; Crozier, T.W.M.; Greenwood, E.J.D.; Lehner, P.J.; Wrigh, G.J. CD147/EMMPRIN, Acts as a Functional Entry Receptor for Measles Virus on Epithelial Cells. *Scientific Reports*. **2021**, *11*, 413, https://doi.org/10.1128/JVI.02168-09 .
17. Behl, T. *et al*., CD147-spike protein interaction in COVID-19: Get the ball rolling with a novel receptor and therapeutic target. *Sci. Total Environ*. **2022**, *808*, 152072, https://doi.org/10.1016/j.scitotenv.2021.152072 .
18. Radzikowska, U. Distribution of ACE2, CD147, CD26, and other SARS-CoV-2 associated molecules in tissues and immune cells in health and in asthma, COPD, obesity, hypertension, and COVID-19 risk factor Basic and Translational. *Allergy Immunology*. **2020**, *75*, 2829-2845, https://doi.org/10.1111/all.14429 .
19. Towler, P.; Staker, B.; Prasad, S.; Menon, S.; Tang, S.; Parsons, J.; Ryan, T.; Fisher, D.; Williams, M.D.; Dales, N.A.; Patane, M.A; Pantoliano, M.W. ACE2 X-ray structures reveal a large hinge-bending motion important for inhibitor binding and catalysis. *J Biol Chem*. **2004**, *279*, 17996-18007, https://doi.org/10.1074/jbc.M311191200 .
20. Zhang, M.Y.; Lin, P.; Zhu, P.; Chen, Z.N.; Crystal structure of CD147 C2 domain in complex with Fab of its monoclonal antibody. **2017**, https://doi.org/10.2210/pdb5x4g/pdb .
21. Yuan, M.; Wu, N.C.; Zhu, X.; So, L; LvMok, H.; Wilson, I.A.; A highly conserved cryptic epitope in the receptor binding domains of SARS-CoV-2 and SARS-CoV. *Science*. **2020**, 368, 630-633, https://doi.org/10.1126/science.abb7269 .
22. BIOVIA, Dassault Systèmes, BIOVIA Discovery Studio Academic Research Suite, San Diego: Dassault Systèmes, 2021.
23. Vilar, S.; Cozza, G.; Moro, S.; Medicinal chemistry and the molecular operating environment (MOE): application of QSAR and molecular docking to drug discovery. *Curr. Top. Med. Chem*. **2008,** 8, 1555–1572. doi: 10.2174/156802608786786624.
24. Yan, Y.; Tao, H.; He, J.; Huang, S.Y.; The HDCK Server for Integrated Protein-Protein Docking. *Nature Protocol*s. **2020**, *15*, 1829-1852, https://doi.org/10.1038/s41596-020-0312-x .
25. Yan, Y.; Zhang, D.; Zhou, P.; Li, B.; Huang, S.Y. HDOCK: a web server for protein-protein and protein-DNA/RNA docking based on a hybrid strategy. *Nucleic. Acids.Res*. **2017**, *45*, 365–373, https://doi.org/10.1093/nar/gkx407 .
26. Weng, G.; Wang, E.; Wang, Z.; Liu, H.; Zhu, F.; Li, D.; Hou, T.; HawkDock: a web server to predict and analyze the protein–protein complex based on computational docking and MM/GBSA. *Nucleic Acids Res*. **2019**, *47*, 322–330, https://doi.org/10.1093/nar/gkz397 .
27. Van Zundert, G.C.P. *et al*. The HADDOCK web server: user-friendly integrative modeling of biomolecular complexes. *J. Mol. Biol.* **2016**, *428*, 720–725, https://doi.org/10.1016/j.jmb.2015.09.014 .
28. Xue L.C.; Rodrigues J.P.; Kastritis., P.L.; PRODIGY: a web server for predicting the binding affinity of protein–protein complexes. *Bioinformatics.* **2016**, *32*, 3676–3678; https://doi.org/10.1093/bioinformatics/btw514 .
29. Battle, G.; PDBePISA: Identifying and interpreting the likely biological assemblies of a protein structure, Chemistry. **2016**, https://doi.org/10.6019/TOL.PDBeP-t.2014.00001.1 .
30. Dafydd, J.; Student Tutorial for PyMOL: for educational use Visualising proteins using molecular graphics. Protein Crystallography. **2002**, *40*, 82-92, https://doi.org/10.13140/RG.2.2.33676.64641 .
31. Kurcinski, M.; Oleniecki, Kuriata, T.; M.P.; Kolinski, A.; Kmiecik, S. CABS-flex standalone: a simulation environment for fast modeling of protein flexibility. *Bioinformatics*. **2019**, *35*, 694–69, https://doi.org/10.1093/bioinformatics/bty685 .